JOURNAL OF combinatorial CHEMISTRY

Article

Understanding Supported Reactions in Spherical Compartments: A General Algorithm To Model and Determine Rate Constants, Diffusion Coefficients, and Spatial Product Distributions

Hans-Joachim Egelhaaf, and Jrg Rademann

J. Comb. Chem., **2005**, 7 (6), 929-941• DOI: 10.1021/cc050015z • Publication Date (Web): 13 September 2005

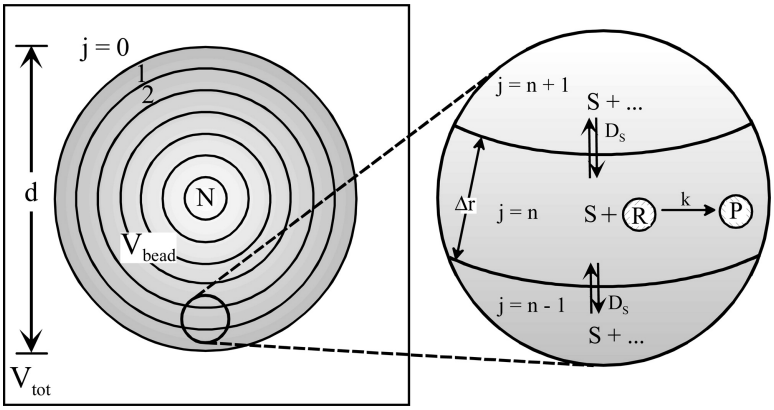

More About This Article

Additional resources and features associated with this article are available within the HTML version:

- Supporting Information
- Access to high resolution figures
- Links to articles and content related to this article
- Copyright permission to reproduce figures and/or text from this article

View the Full Text HTML

Journal of Combinatorial Chemistry is published by the American Chemical Society.
1155 Sixteenth Street N.W., Washington, DC 20036

Understanding Supported Reactions in Spherical Compartments: A General Algorithm To Model and Determine Rate Constants, Diffusion Coefficients, and Spatial Product Distributions

Hans-Joachim Egelhaaf[‡,⊥] and Jörg Rademann*[,†,§]

Medicinal Chemistry, Leibniz Institute for Molecular Pharmacology (FMP), Berlin, Germany, Institute for Physical Chemistry, Eberhard-Karls University Tübingen, Tübingen, Germany, and Institute for Chemistry, Free University Berlin, Berlin, Germany

Received February 3, 2005

A general algorithm allowing the numerical modeling of the time and space dependence of product formation in spherical reaction volumes is described. The algorithm is described by the complete set of mass balance equations. On the basis of these equations, the effects of the diffusion coefficient, reaction rate, bead size, reagent excess, and packing density of the resin beads on the overall reaction rates are determined for second-order reactions. Experimental data of reaction progress are employed to calculate reaction rates and diffusion coefficients in polymer-supported reactions. In addition, the conditions for shell-like product formation are determined, and various strategies for the radial patterning of resin beads are compared. The effect of diffusion on polymer-supported enzyme-catalyzed reactions of the Michaelis−Menten type is treated, as well. Finally, the effects of typical nonideal solid-phase phenomena, namely, the inhomogeneity of rate constants and the concentration dependence of diffusion coefficients, on overall rates are discussed.

Introduction

Reactions in inhomogeneous media are ubiquitous in chemical and in biological systems. All processes in compartmentalized reactors, such as cells and cellular organelles, belong to this class. As one prominent example, during recent decades, polymer-supported reactions have developed into an area of growing significance. They have changed the manner of synthetic practice, and they have triggered the evolution of combinatorial chemistry.[1−3]

Despite intense research efforts, the profound understanding of solid phase and other heterogeneous transformations is still rather limited. The rational planning of polymer-supported reactions is mostly based on empirical knowledge collected over the years. Often, even experienced organic chemists consider polymer beads as black boxes. A general rationalization of the progress of polymer-supported reactions has not yet been accomplished.

Over recent years, significant progress has been achieved in the on- and off-bead analysis of polymer-supported reactions;[4−11] however, without a quantitative model at hand, the analysis of experimental data with respect to optimization of processes and materials is difficult. A computational model allowing for the simulation of polymer-supported reactions using experimentally accessible parameters would be of great practical value, for example, in the rationalization of matrix effects on polymer-supported reactions. Such a method could also be used for the determination of parameters that are not accessible experimentally by fitting the data to the model.

There have been a series of attempts to calculate reaction rates in heterogeneous systems. Most of these calculations deal with heterogeneous catalysis. It was recognized long ago that realistic modeling of chemical reactions in inhomogeneous media, for example, of solid-phase synthesis, heterogeneous catalysis, or cellular reactions, needs to account for both reaction and simultaneous diffusion.[12−22] Simpler models apply only in cases in which either of these processes is much faster than the other one. When diffusion is fast compared to reaction, the overall reaction kinetics are "solution-like", even when the actual reaction rates are usually significantly reduced in comparison to those in solution.[7] Reactions which are dominated by uptake of reactant into the microreactors have been described successfully by diffusive mass transfer into spheres.[23]

For simple reaction types and special boundary conditions, the material balance equations for diffusion-reaction systems have been solved analytically.[12,14,15,23] The most well-known among these expressions is that derived by Thiele for first- and second-order reactions in porous catalysts.[10] Assuming that steady-state conditions apply during the reaction, the dimensionless Thiele modulus is obtained

$$\mathrm{TM} = \frac{d}{2}\sqrt{\frac{a_S}{pD}} \tag{1}$$

where d is the diameter of the catalyst grains, a_S is the activity of the unit internal surface of the pores, p is the hydraulic

* To whom correspondence should be addressed. Leibniz Institute for Molecular Pharmacology (FMP), Robert-Rössle-Str. 10, 13125 Berlin, Germany. Phone: (Int.) 49 30 94793275. Fax: (Int.) 49 30 94793280. E-mail: rademann@fmp-berlin.de.

† Leibniz Institute for Molecular Pharmacology.

‡ Eberhard-Karls University Tübingen.

§ Free University Berlin.

⊥ Present address: Dipartimento di Fisica, Politecnico di Milano, Italy.

10.1021/cc050015z CCC: $30.25
Published on Web 09/13/2005

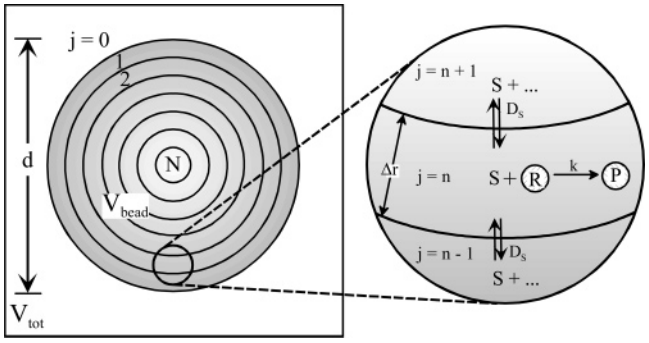

Figure 1. Concept of the algorithm. The resin beads of diameter d and volume V_{bead} and the surrounding homogeneous solution completely fill the reaction vessel of volume V_{tot}. A single bead is divided into N shells of thickness Δr. The mobile reactant, S, diffuses between the shells with diffusion coefficient D_S and undergoes a reaction with the polymer-supported reactant R with the second-order rate constant, k, yielding polymer-supported product P.

radius of the pores, and D is the diffusion coefficient of the reactant. If TM $\gg$ 1, the reaction is diffusion-controlled; i.e., the reaction rate is proportional to the reciprocal of the grain size. For TM $\ll$ 1, the reaction is activation-controlled; i.e., the reaction rate is independent of the grain size.

Because analytical solutions are only accessible for simple reaction types and special boundary conditions, their application is severely limited. Therefore, a number of diffusion-reaction systems have been treated by numerical solution of the corresponding sets of mass balance equations using finite difference[17,18,20,24] and finite element[25,26] techniques. However, these methods have not yet been applied to the systematic modeling of matrix effects on polymer-supported reactions on resin beads.

Here, we wish to introduce a general algorithm that allows for the numeric modeling of the time- and space-dependence of product formation in spherical reaction volumes under almost any set of boundary conditions. We will first describe the algorithm by introducing the complete set of mass balance equations. On the basis of these equations, the effects of diffusion coefficient, reaction rate, bead size, reagent excess, and packing density of the resin beads on the overall reaction rates are described for second-order reactions and applied to the interpretation of experimental results for solid-phase reactions. Subsequently, different strategies for radial patterning of resin beads are compared. The effect of diffusion on polymer-supported enzyme catalyzed reactions of the Michaelis−Menten type is treated, as well. Finally, the effects of typical nonideal solid-phase phenomena, namely, distributions of rate constants and concentration dependence of diffusion coefficients, on overall rates are discussed.

Results and Discussion

Description of the Algorithm. For the derivation of the algorithm, it is assumed that polymer-supported reactions are described appropriately by the diffusion of a reactant in solution (S) to the reactive sites (R) immobilized inside the resin beads, followed by a second-order reaction, yielding an immobilized reaction product (P): R + S → P (see Figure 1). The rate of this reaction is calculated by solving the mass balance eq 2 for the concentration of S, c_S, at any time, t, and any distance, r, from the bead center.

$$\frac{\partial c_S(r,t)}{\partial t} = D_S(r,t)\cdot\frac{\partial^2 c_S(r,t)}{\partial r^2} - k(r,t)c_S(r,t)c_R(r,t) \quad (2)$$

The first term on the right-hand side of eq 2 describes the diffusion of S inside the bead, expressed by Fick's second law. The second term describes the consumption of S by the reaction with the immobilized reactants, R. In heterogeneous systems, the diffusion coefficient, D_S, and the second-order rate constant, k, are generally time- and space-dependent.

General analytical solutions of eq 2, that is, of the combination of diffusion processes with subsequent chemical transformations, are not available. Thus, we use numerical methods to solve the corresponding set of difference equations. This offers the advantage of the algorithm's being easily adaptable to changing boundary conditions and even different reaction types, for example, transformations involving polymer-supported catalysts.

The concept of the algorithm is visualized in Figure 1. A resin sphere and the surrounding solution are contained in a total reaction volume, V_{tot}, of which the resin sphere occupies a fraction X. The resin sphere is divided into N sufficiently thin concentric spherical shells, $j = 1, ..., N$. For every shell, j, the change of concentration of S, $\Delta c_S(j, t)$, during the sufficiently small time interval Δt is calculated. The concentration changes caused by diffusion and reaction, $\Delta c_{s,diff}(j, t)$ and $\Delta c_{s,react}(j, t)$, respectively, contribute additively to $\Delta c_S(j, t)$. Loss or gain of S resulting from diffusion to or from the two adjacent shells is obtained by applying Fick's first law, inserting the diffusion coefficient D_S of S in the resin (eq I). (Roman numerals refer to equations in the Computational Section.) Partitioning of S between solution and bead is accounted for by introducing the partition coefficient α_S (eqs Ib and c). The decrease of concentration due to the reaction of S with R is calculated according to a second-order rate law (eq II), inserting the rate constant k. After the concentrations of S and R, $c_S(j)$ and $c_R(j)$, have been calculated for all shells (eqs III), the procedure is repeated using the result of time step $t \rightarrow t + \Delta t$ as input for the calculation of time step $t + \Delta t \rightarrow t + 2\Delta t$, until the desired maximum reaction time has been reached. In this simple model, a polymer-supported reaction is reduced to three characteristic parameters: the second-order rate constant, k, the diffusion coefficient, D_S, and the diameter of the resin sphere, d. Additional parameters are introduced to describe variable reaction conditions: the volume fraction occupied by the resin, $X = V_{bead}/V_{tot}$, and the initial concentrations of S and R, c_{S0} and c_{R0}, respectively.

The following boundary conditions apply during the simulations: The polymer-bound reactant R is homogeneously distributed in spherical resin particles which are dispersed in a homogeneous solution of the reactant S. That the polymer-bound rectants are, indeed, homogeneously distributed has been shown experimentally in several cases, for example, by Raman[6] and fluorescence microscopy.[5,27] The suspension is ideally stirred; i.e., the concentration of S

outside the resin is uniform at all times;[28,40] the initial concentration of S inside the beads is 0. The diffusion coefficient and rate constant are independent of the position in the resin bead. The diameter of the beads remains constant throughout the reaction. In addition, coated particles may be treated by slightly changing the boundary conditions: a certain radius, r_{max}, is chosen so that $d/2 - r_{max}$ is the thickness of the active layer, which is constituted by shells $j = 1$ to j_{max}. The concentration of polymer-bound reactant in the inactive core is set to c_{R0} ($r < r_{max}$) = 0. If it is desired that the core of the particle be inaccessible to the mobile reactant S, diffusion of S through the sphere with radius r_{max} is supressed by setting the surface area between shell j_{max} and the core to 0, that is, $A_{j,max+1} = 0$.

To gain reliable information from the comparison between experiments and simulations, the number of adjustable parameters in the simulations should be kept as small as possible. As many reaction parameters as possible must either be set to a fixed value by controlling the reaction conditions or they must be determined by independent physicochemical methods. One of the most important requirements is to keep the temperature of the reaction system constant. This is easy to achieve for the mobile phase, whereas local temperature gradients inside the beads cannot be completely avoided. However, for the examples given below, temperature changes are so small that even for large values of reaction enthalpies, they do not change the reaction rates significantly. Thus, for the sake of clarity, temperature changes are not considered in this article. A further requirement pertains to the homogeneity of the beads and their physicochemical properties. For example, D_S and k should be independent of time and space. This condition is not easy to maintain in practice because the properties of the resin may be changed appreciably by the reaction, especially for highly loaded resins.[29] How local and spatial variations of k and D_S can be dealt with will be shown in part 3 of the next section, below. The distribution of reactive sites R inside the beads should be homogeneous, which may be monitored by some spectroscopic method, for example, fluorescence or Raman microscopy.[5,6] Ideal stirring conditions have to be provided, either by vivid stirring or shaking or by rapid flow. The starting point of the reaction should be well-defined in time. In the case of reactions at elevated temperatures, this implies that the target temperature has to be reached very quickly. In addition, the beads should be preswollen by the solvent in which the reaction occurs. Significant contributions of anomalous diffusion should be avoided.

Application of the Algorithm. In the following, the algorithm described in the previous section will be employed to model characteristic situations relevant to the synthetic chemist and biochemist. We concentrate mainly on reaction conditions which are typical for polymer-supported organic synthesis (as, e.g., the large excess of mobile reactant with respect to resin-bound reactant, which is commonly employed to achieve nearly complete conversion of the latter). The effects of D_S, k, d, X, and reagent excess on the overall rate of the polymer supported reaction will be described. Finally, examples from the literature will be discussed on the basis of this model.

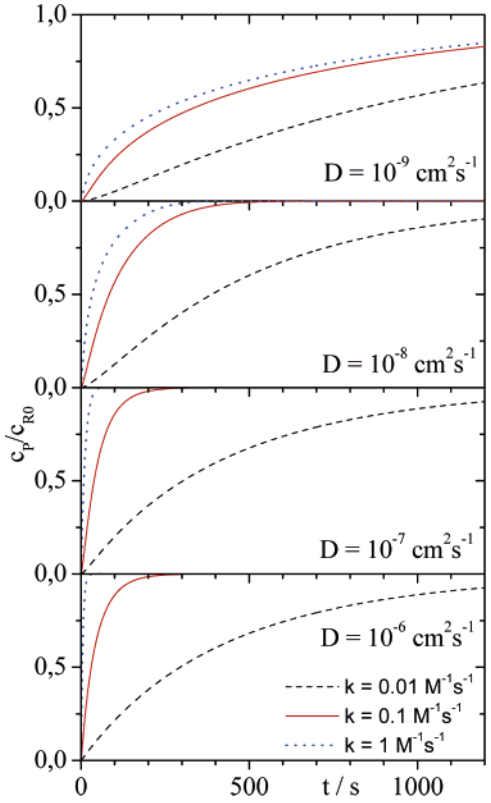

Figure 2. Simulated time traces of product formation normalized to the initial concentration of reactant R (c_P/c_{R0} corresponds to the fraction of reacted polymer-supported reaction sites and, thus, gives the conversion of R) during polymer-supported reactions with different diffusion coefficients, D, and second-order rate constants, k. The other parameters are kept constant: $d = 100$ μm, $X = 0.5$, $c_{R0} = 0.05$ M, $c_{S0} = 0.25$ M.

1. The Effect of Diffusion Coefficient and Second-Order Rate Constant on the Overall Reaction Rate. The graphs in Figure 2 show the relative product yield, $c_P(t)/c_{R0}$, for the reaction S + R → P in beads of $d = 100$ μm as a function of reaction time for different combinations of k and D. For the bimolecular reaction rate constant, k, values of 1, 0.1, and 0.01 M^{-1} s^{-1} are chosen. The diffusion coefficient is varied from $D = 10^{-9}$ cm^2 s^{-1} to $D = 10^{-6}$ cm^2 s^{-1}.

Although diffusion coefficients of typical reactants in solution vary between values such as $D_0 = 0.65 \times 10^{-6}$ cm^2 s^{-1} for the protein BSA in water[30] and $D_0 = 13.5 \times 10^{-6}$ cm^2 s^{-1} for methyl red in benzene,[31] they are significantly reduced in polymer gels. In many cases of solvent-penetrated polymer gels at high solvent concentrations, the diffusion coefficient of the solute decreases exponentially with the volume fraction, φ, of the polymer. For a given value of φ, the reduction of D depends on the type of polymer, the solute size, the solute concentration, and possible specific interactions between solute and polymer (for further details see, e.g., the review article by Masaro and Zhu[32]). In well-swollen beads, the volume fraction of the polymer usually is $\varphi \approx 0.2-0.4$. For small and medium-sized organic reagents, this leads to a reduction of the diffusion coefficient by a factor of typically 3−6[32] (e.g., the diffusion coefficient of BOC−Phe is reduced from $D_0 = 4.8 \times 10^{-6}$ cm^2 s^{-1} in DMF bulk solution to $D_e = 0.9 \times 10^{-6}$ cm^2 s^{-1} in DMF-swollen polystyrene beads).[33] More dramatic decreases are observed for higher values of φ, high degrees of cross-linking, larger

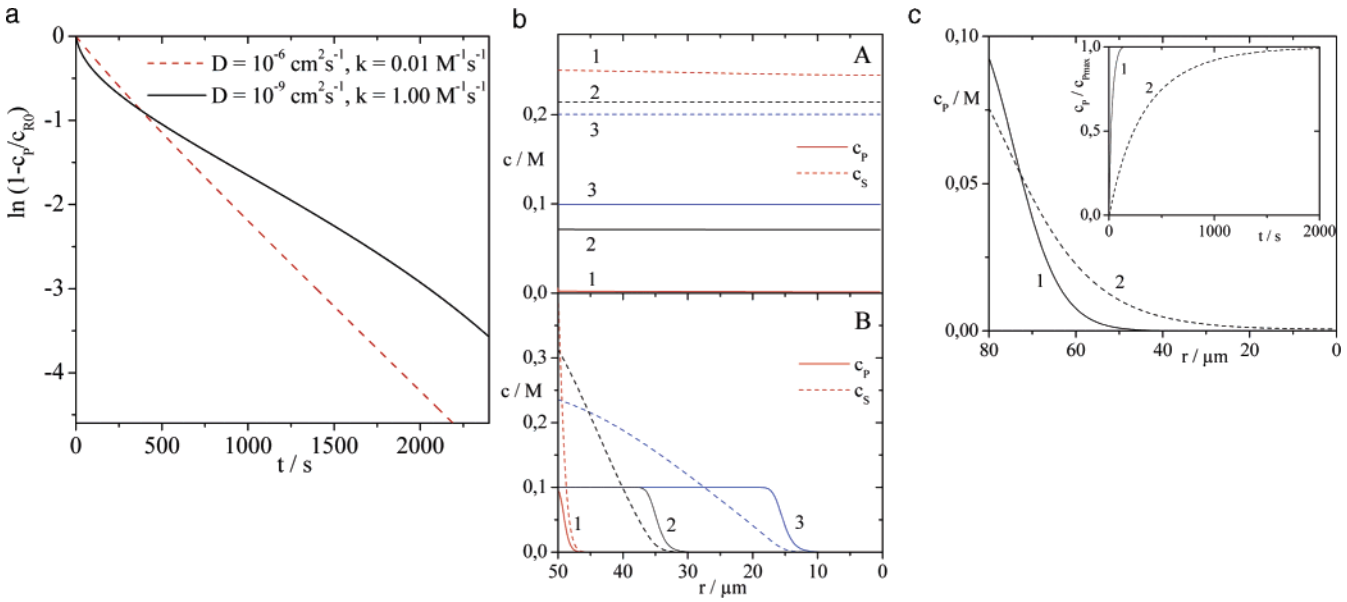

Figure 3. (a) Semilogarithmic plots of the reagent conversion ($1 - c_P/c_{R0}$ corresponds to the fraction of nonreacted polymer-supported reaction sites) vs time for two extreme values of the ratio D_S/k. (b) Radial patterning of beads by solid-phase reactions: Concentration profiles of product P (solid line) and mobile reactant S (broken line) along the radius of the bead ($r = 0$ corresponds to the bead center) at different times after the start of the reactions. (1) $t = 10$ s, (2) $t = 400$ s, (3) $t = 2400$s. A: $k = 0.01$ M^{-1} s^{-1}, $D_S = 10^{-6}$ cm^2 s^{-1}. B: $k = 1.00$ M^{-1} s^{-1}, $D_S = 10^{-9}$ cm^2 s^{-1}. Please note that curve 3 corresponds to 97% completion of the reaction. (c) Radial patterning of polymer beads by reactions with substoichiometric reagent. Concentration profiles for two polymer-supported reactions with different initial concentrations of S but otherwise equal parameters ($k = 1$ M^{-1} s^{-1}, $D_S = 10^{-7}$ cm^2 s^{-1}, $X = 0.091$, $c_{R0} = 0.01$ M). (1) $c_{S0} = 0.2$ M, reaction quenched after $t = 10$ s; (2) $c_{S0} = 0.003$ M, reacted until completion. Inset: time courses of the reactions (conversion vs time).

solute sizes, and strong solute−polymer interactions[32,34] (e.g., the diffusion coefficient of rhodamines is reduced from $D_0 = 2.8 \times 10^{-6}$ cm^2 s^{-1} in water[35] to $D_e \approx 10^{-7}$ cm^2 s^{-1} in solvent-swollen polymer beads[36] and to $D_e \approx 5 \times 10^{-10}$ cm^2 s^{-1} in silica sol−gel materials).[23,37,38]

For the bead size of $d = 100$ μm considered here, the effective rate of the overall reaction shows a pronounced dependence on both k and D_S. Although the reactions do not follow simple rate laws (see below), the time traces can be fitted to first-order rate laws (eq 3) in fair approximation, because the mobile reactant S is present in 5-fold excess in the overall reaction.

$$-\frac{dc_R}{dt} = k'c_R \qquad (3)$$

For the fastest rate constant of $k = 1$ M^{-1} s^{-1} the exponential fit yields pseudo-first-order effective rate constants for the overall reaction of $k' = 0.2$, 0.12, 0.014, and 0.0013 s^{-1}, for diffusion coefficients of $D_S = 10^{-6}$, 10^{-7}, 10^{-8}, and 10^{-9} cm^2 s^{-1}, respectively. For the smallest second-order rate constant of $k = 0.01$ M^{-1} s^{-1}, pseudo-first-order rate constants of $k' = 0.002$ s^{-1} are obtained for $D_S = 10^{-6}$–10^{-8} cm^2 s^{-1}. Only for the smallest diffusion coefficient of $D_S = 10^{-9}$ cm^2 s^{-1} is a slightly reduced value of $k' = 0.0009$ s^{-1} obtained. This means that for beads of $d \leq 100$ μm, the effect of diffusion on the overall reaction rate is negligible, provided second-order rate constant and diffusion coefficient do not take on extreme values, that is, as long as $k \leq 0.1$ M^{-1} s^{-1} and $D_S \geq 10^{-8}$ cm^2 s^{-1}.

As already mentioned above, closer inspection of the time traces reveals that the reactions of Figure 2 do not follow simple rate laws. The exponential fits, for which the results are given above as measures for the overall reaction rates, are only more or less satisfactory approximations. Figure 3a shows a semilogarithmic plot of two extreme combinations of k and D. For case 1 ($k = 0.01$ M^{-1} s^{-1} and $D_S = 10^{-6}$ cm^2 s^{-1}), the exponential fit curve reproduces the simulation very well. Case 2 ($k = 1$ M^{-1} s^{-1} and $D = 10^{-9}$ cm^2 s^{-1}) yields strong deviations from exponentiality. After a rapid start, the reaction slows down appreciably.

This dependence of kinetics on the ratio D_S/k can be rationalized by considering the temporal developments of the concentration profiles of S and R during the reaction (Figure 3b). Case 1 may be regarded as a two-step reaction, in which the beads are quickly penetrated by the reactant S in a first step, which is followed by a homogeneous pseudo-first-order reaction between S and R. In case 2, the reaction starts with a rate which is determined by the second-order rate constant, k, because the concentration of S in regions of nonreacted R in the bead is high. This is due to relatively fast diffusion at the beginning of the reaction, which in turn is a consequence of the large concentration gradient of S in the outer regions of the beads at that time. Because S is consumed rapidly after having reached a nonreacted region of the bead, a rather sharp reaction front is formed. The concentration gradient of S becomes smaller as the reaction front proceeds into the bead. Consequently, diffusion slows down, which results in a decreasing overall reaction rate.

The simulation of concentration profiles may be helpful in the task of radial patterning of resin beads. Radial patterning (shell formation) is achieved by one of the following strategies: (a) adding S in subequivalent amounts and reacting the mixture until completion[5] or (b) quenching the resin-modifying reaction after the appropriate time span.

Polymer spheres with two to five differently functionalized concentric shells have been produced via a series of protection/deprotection reactions.[39] At first glance, strategy (a) seems to be less favorable, because the reaction takes much longer, and the resulting boundary between modified and unmodified regions is more diffused (Figure 3c). However, in practice, quenching of the modifying reaction will always involve a diffusion process (either of a quenching agent into the bead or of the reactant out of the bead). Consequently, the resulting product profile will not be as steep as that given by curve 1 in Figure 3c.

The profiles in Figure 3b show that both strategies require the formation of sufficiently sharp reaction fronts. This, in turn, requires the rate of diffusion of S,

$$\left(\frac{\mathrm{d}N_{\mathrm{diff}}}{d\mathrm{t}}\right)_{r,t} = D_{\mathrm{S}}A(r)\left(\frac{\mathrm{d}c_{\mathrm{S}}}{\mathrm{d}r}\right)_{r,t} \tag{4a}$$

into any shell at distance r from the center to be much smaller than the rate of its consumption,

$$\left(\frac{\mathrm{d}N_{\mathrm{react}}}{\mathrm{d}t}\right)_{r,t} = kc_{\mathrm{R}}(r,t)c_{\mathrm{S}}(r,t)\,\mathrm{d}V \tag{4b}$$

in this shell of volume dV:

$$kc_{\mathrm{R}}(r,t)c_{\mathrm{S}}(r,t)\,\mathrm{d}V \gg D_{\mathrm{S}}A(r)\left(\frac{\mathrm{d}c_{\mathrm{S}}}{\mathrm{d}r}\right)_{r,t} \tag{4c}$$

We require the reaction front to be not wider than $\Delta r = d/10$, which yields a maximum value of $\Delta V \approx 4\pi r^2 d/10$ for the active reaction volume at a distance r from the bead center. Both rates constantly change as the reaction front proceeds toward the center of the bead. As evident from Figure 3b, the concentration gradient of S is approximately linear if S is consumed more rapidly than it is provided by diffusion. We arbitrarily consider the situation when half of the immobilized reactant has reacted, that is, when the reaction front has reached $r = r' \approx 0.8d/2$

$$kc_{\mathrm{R}}(r',t)\frac{c_{\mathrm{S}}(d/2,t)}{5}A(r')\frac{d}{10} \gg D_{\mathrm{S}}A(r')\frac{c_{\mathrm{S}}(d/2,t)}{0.1d} \tag{5a}$$

$$\frac{kc_{\mathrm{R}}d^2}{500D_{\mathrm{S}}} \gg 1 \tag{5b}$$

This expression serves as a rule of thumb for the formation of sharp reaction fronts. It is analogous to Thiele's modulus, however, with an important difference. Thiele's modulus was derived for catalysts, for which a steady state is maintained throughout the reaction. In our case, the concentration gradient of S decreases as the immobilized reactant is consumed. Therefore, no steady state is reached during the reaction. The diffusion gradient is steeper at the beginning of the reaction and decreases with time, whereas the width of the reaction front remains almost constant. Thus, the modulus will be larger in the beginning than toward the end of the reaction.

This modulus may also serve as a guideline to distinguish between diffusion-controlled ($kc_{\mathrm{R}}d^2/500D_{\mathrm{S}} \gg 1$) and activation-controlled ($kc_{\mathrm{R}}d^2/500D_{\mathrm{S}} \ll 1$) reactions.

Diffusion coefficients may be controlled by using solvents of different swelling abilities, but care must be taken that there is no concomitant variation of the rate constant.

2. The Effect of Bead Size on the Overall Reaction Rate. The elucidation of the impact of bead size on the progress of solid phase reactions has been an issue of many experimental and theoretical investigations. Different cases have been observed. No dependence of reaction rate on bead size has been found for a comparably slow alkylation of a phenolate, monitored by spatially resolved resin bead analysis.[28] In addition, no bead-size dependence was observed for the oxidation of benzyl chloride to benzaldehyde by using chromate salts supported on a DVB cross-linked polystyrene.[40] However, for many reactions involving polymer-supported catalysts, it has been found that the overall reaction rate is a function of inverse bead size.[12,41−43] Recently, for the aminomethylation of modified porous silica, a dependence of the overall reaction rate on d^{-2} was reported.[23]

These different cases may be understood by simple kinetic considerations, based on the arguments of the preceding section. If diffusion is much faster than reaction, that is, $D_{\mathrm{S}}/kc_{\mathrm{R}}d^2 \rightarrow \infty$, significant reaction starts only after the beads have been homogeneously penetrated by mobile reactant S. The reaction rate will thus be independent of bead size. If, on the other hand, diffusion is much slower than reaction, that is, $D_{\mathrm{S}}/kc_{\mathrm{R}}d^2 \rightarrow 0$, mobile reactant S is consumed as soon as it enters regions with active immobilized reactant R. In catalysts, this leads to the formation of a steady state, which involves a linear concentration gradient of S throughout the reaction. Thus, the mass of S entering the beads per unit time is proportional to the total surface area of all beads in the reaction system, which is proportional to $1/d$ if the amount of R is kept constant. For polymer-supported synthesis, where S is usually added in excess over R, the diffusion front moves from the surface of the bead to its center as the reaction proceeds. Therefore, the concentration gradient and, thus, the rate of diffusion decrease during the reaction. Under these conditions, the rate of diffusive mass uptake into an ensemble of spheres scales with d^{-2} at constant total volume of the sphere ensemble.[44] The same is therefore true for the overall reaction rate.

Although these simple considerations allow one to assess the expected bead size dependence of the reaction rate, the algorithm presented in part 1 is capable of providing the product distribution at any time and at any location for any combination of diffusion coefficient, reaction rate, and bead size. Figure 4 gives an overview of the effect of particle size on the reaction half time. Three different cases are presented here. Reactions with high second-order rate constants and relativey small diffusion coefficients show a strongly superlinear dependence of the effective reaction rate on bead diameter. The example shown in Figure 4a ($k = 1$ $\mathrm{M^{-1}\ s^{-1}}$, $D = 5 \times 10^{-8}$ $\mathrm{cm^2\ s^{-1}}$) is very close to ideal diffusion control, resulting in a fairly linear plot of reaction half time vs square of the bead diameter. Increasing the diffusion coefficient to $D = 10^{-6}$ $\mathrm{cm^2\ s^{-1}}$ results in a >10-fold faster reaction for the 500-μm beads, whereas the effective rate for beads of $d = 20$ μm increases by only 50% (Figure 4b). For reactions with small reaction rates and large

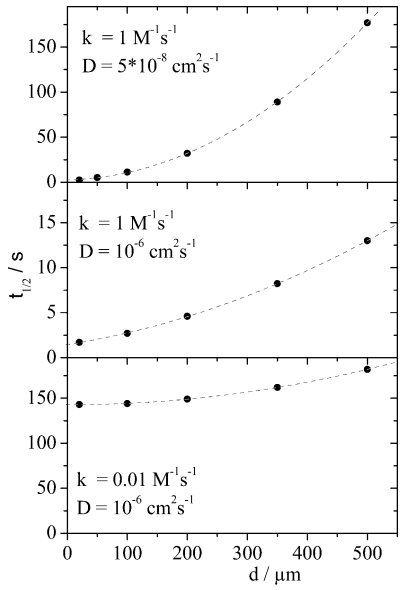

Figure 4. Calculated reaction half-lives, $t_{1/2}$, as a function of bead diameter, d, for three polymer-supported reactions with different combinations of k and D_S (note the different ordinate scales). The remaining parameters are kept constant: $X = 0.2$, $c_{R0} = 0.05$ M, $c_{S0} = 0.5$ M. The polynomial fit curves are guides to the eye.

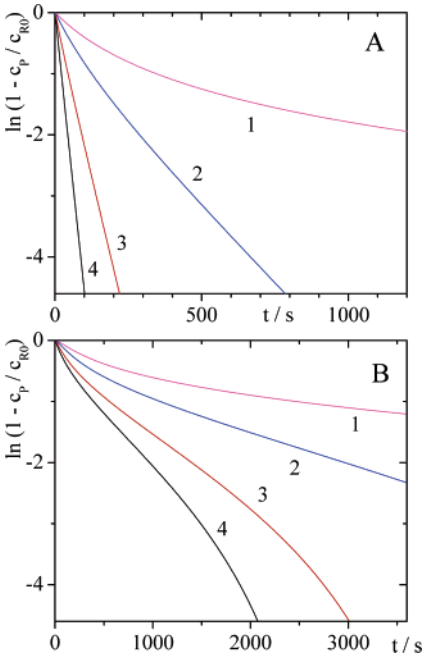

Figure 5. Semilogarithmic plots of the time traces of polymer-supported reactions ($c_{R0} = 0.05$ M, $k = 0.1$ M^{-1} s^{-1}, $X = 0.5$) on beads of diameter $d = 100$ μm for two different diffusion coefficients (A, $D = 10^{-6}$ cm^2 s^{-1}; B, $D = 10^{-9}$ cm^2 s^{-1}). Reaction progress is given in fractions of nonreacted polymer-supported reactants ($1 - c_P/c_{R0}$). For each diffusion coefficient, the traces were simulated for initial reactant concentrations of $c_{S0} = 0.05$ M (curve 1), $c_{S0} = 0.10$ M (curve 2), $c_{S0} = 0.25$ M (curve 3), and $c_{S0} = 0.50$ M (curve 4).

diffusion coefficients ($k = 0.01$ M^{-1} s^{-1}, $D = 10^{-6}$ cm^2 s^{-1}), the dependence of the effective reaction rate on bead diameter is almost negligible (Figure 4c).

3. The Effect of Reagent Excess on the Overall Reaction Rate. In solid-phase synthesis, the mobile reactant is usually added in excess of the immobilized reaction sites to maximize the conversion of the latter. The relative excess of S over R affects not only the yield, but also the rate of the overall reaction. Reactions that are characterized by a high ratio of D_S/kc_Rd^2 (see Figure 5a, where $D_S = 10^{-6}$ cm^2 s^{-1} and $k = 0.1$ M^{-1} s^{-1}) show a concentration dependence that is very similar to that of homogeneous solutions. If S is present in equimolar amounts, the reaction rate obeys a second-order rate law in good approximation. For the example shown in Figure 5a, it takes $t = 200$ s for 50% completion and $t = 2300$ s for 92% completion of the reaction. Upon doubling the amount of S, these time spans are reduced to $t = 82$ and 380 s, respectively. Addition of S in 5-fold excess over R yields a pseudo-first-order reaction with a reaction half time of $t_{1/2} = 30$ s, whereas 10-fold excess results in $t_{1/2} = 15$ s. These half-lives are practically the same as for the corresponding homogeneous reactions.

Reactions with smaller ratios of D_S/kc_Rd^2 (see Figure 5b, where $D_S = 10^{-9}$ cm^2 s^{-1} and $k = 0.1$ M^{-1} s^{-1}), for which the rates are dominated by diffusion and the kinetics, thus, significantly deviate from first order, also show a pronounced dependence on the concentration of the mobile reactant S. For the example shown in Figure 5b, increasing the concentration of S from an equimolar ratio to 2-, 5-, and 10-fold excess over R causes a reduction of the reaction half time from $t_{1/2} = 1250$ s to $t_{1/2} = 620$, 335, and 240 s, respectively. In the case of diffusion-dominated reactions, the enhancement of the reaction rate with increasing concentration of S is due to the larger concentration gradient of S, which in turn leads to an increased flux of mobile reactant into the resin beads. As demonstrated by Figure 5b, this dependence of reaction rates on mobile reactant concentration is more pronounced for small concentrations of S.

4. The Effect of the Ratio of Solvent and Bead Volumes on the Overall Reaction Rate. The fraction X of the reaction volume that is occupied by the resin beads also affects the reaction rates. Figure 6 shows the time traces of two reactions with different degrees of diffusion control. The kinetics of each of these reactions has been calculated for both $X = 0.5$, which corresponds to relatively close packing of spheres, as obtained in a flow reactor, and for $X = 0.04$, which is more characteristic of a stirred suspension. As illustrated by the time traces in Figure 6a (for which $D_S = 10^{-8}$ cm^2 s^{-1} and $k = 1$ M^{-1} s^{-1}), the rates of highly diffusion-controlled reactions decrease significantly with decreasing packing density. This effect is due to different concentrations of mobile reactant S in the liquid phase at different packing densities. At low packing densities, the concentration of S in the liquid phase is smaller than at high packing densities, because the total amount of S in the reaction system is the same in both cases. Thus, smaller concentration gradients of S are obtained for smaller values of X, which in turn lead to reduced mass transfer of S into the beads at small packing densities. The lesser the extent to which reactions are limited by diffusion, the weaker is the dependence of their overall reaction rate on X, as demonstrated by the reaction shown in Figure 6b ($D_S = 10^{-7}$ cm^2 s^{-1} and $k = 0.1$ M^{-1} s^{-1}), which is much less sensitive to packing density than its counterpart of Figure 6a. For reactions that are far from diffusion control (e.g., $D_S = 10^{-6}$ cm^2 s^{-1} and $k = 0.01$ M^{-1} s^{-1}), the differences between the time traces calculated for

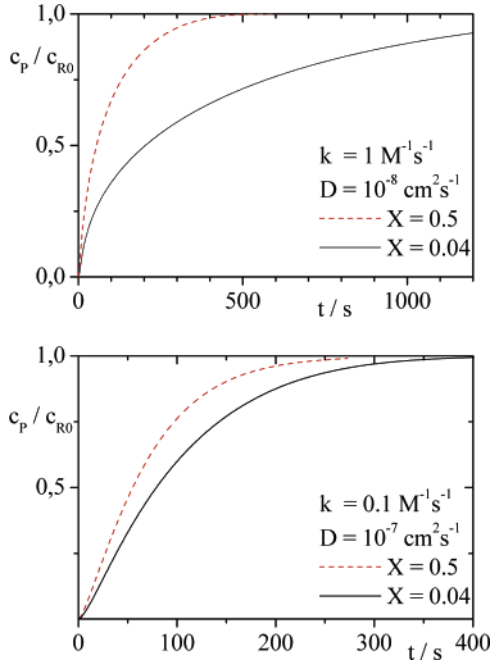

Figure 6. Normalized time traces of product formation (expressed in terms of conversion of polymer-supported reagent, c_P/c_{R0}) during polymer supported-reactions (bead diameter $d = 160$ μm, $c_{R0} = 0.01$ M, $c_{S0} = 0.2$ M) for two different combinations of k and D_S. For each of these cases, the time traces are simulated for two different values of X.

$X = 0.5$ and 0.04 are negligible, because the concentrations of S within the beads are practically the same for both values of X.

5. Simulation of Experimental Kinetic Data of Resin-Supported Reactions. In the following, the model will be applied to the interpretation of experimental data obtained by Li et al.[45] on the effective rate of Knorr attachment onto

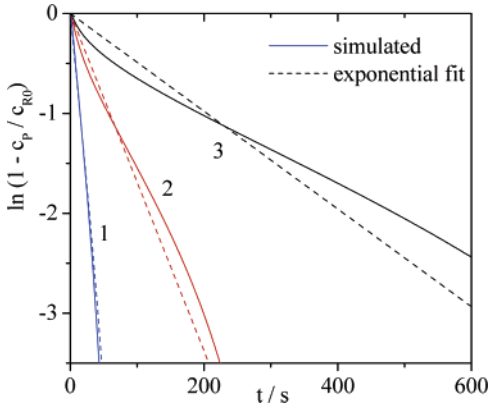

Figure 7. Simulated time traces (solid curves) of product formation (given in fractions of nonreacted polymer-supported reactant, $1 - c_P/c_{R0}$) during Knorr attachment to aminomethyl polystyrene beads of three different sizes. The parameters used in the simulations are listed in Table 1. (1) $d = 80$ μm, (2) $d = 160$ μm, (3) $d = 320$ μm. The dashed curves are exponential fits to the simulations.

aminomethyl polystyrene resins (see Scheme 1). The reaction was carried out on beads of three different sizes under the conditions specified in Table 1. In all three reactions, identical amounts of 0.5 mmol of amino groups (R) were added to 50 mL of 0.2 M solutions of Knorr linker (S) in dichloromethane (thus, due to different loadings of the polystyrene resins with amino groups, the volume fractions X vary with bead size). The authors obtained first-order rate constants k'_{exp} from exponential fits to the experimental data (Table 1). These rate constants decrease significantly with increasing bead size.

We attempted to reproduce the bead-size dependence of the reaction rates by using a single set of k and D_S values in the simulations for all bead sizes. Figure 7 shows the set of simulated time traces obtained for $k = 1.25$ M^{-1} s^{-1} and D_S

Scheme 1. Knorr Linker Attachment Investigated on Six Different Resins[a]

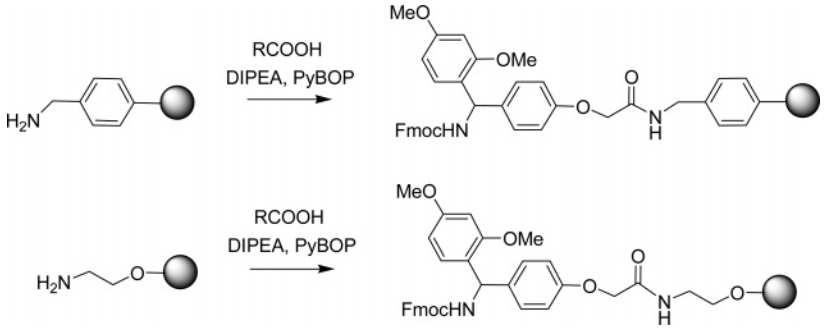

[a] See Table 2.[36] The primary amine is a benzylic amine (top) in the polystyrene resins and the champion resin, and an aliphatic PEG-amine (bottom) in the case of Tentagel and Argogel resins.

Table 1. Parameters Used for the Simulation of the Curves in Figure 7

resin type	d^a, μm	X^a	$c_{R0}{}^a$, M	$c_{S0}{}^a$, M	k, M^{-1} s^{-1}	D, cm^2 s^{-1}	$k'_{exp}{}^b$, s^{-1}	$k'_{sim}{}^b$, s^{-1}
PS	80	0.04	0.01	0.2	1.25	7×10^{-8}	0.077	0.069
PS	160	0.04	0.01	0.2	1.25	7×10^{-8}	0.021	0.017
PS	320	0.1	0.01	0.2	1.25	7×10^{-8}	0.004	0.005
Tentagel	200	0.1	0.01	0.2	1.5	3×10^{-7}	0.06	0.051
Argogel	240	0.063	0.01	0.2	2	6×10^{-7}	0.07	0.076
Champion	160	0.063	0.01	0.2	10	1×10^{-6}	0.4	0.3

[a] The values for the diameters of the swollen beads, d, the volume fractions X, and the initial reactant concentrations c_{R0} and c_{S0} were calculated from the data given in ref 45. The second-order rate constants k and the diffusion coefficients D were used for the simulations. [b] The first-order rate constants, k'_{exp} and k'_{sim}, were obtained from exponential fits to the experimental data[45] and to the simulated curves, respectively.

Scheme 2

$$S_{mob} + R_{stat} \underset{k_{-1}}{\overset{k_1}{\rightleftharpoons}} Z_{stat} \xrightarrow{k_2} P_{mob} + R_{stat}$$

$= 7 \times 10^{-8}$ cm^2 s^{-1}, which is among the closest approximations to the experimental data. To be able to compare experimental and simulated rate constants, exponential curves are fitted to the simulated time traces (Figure 7). The simulated time traces are clearly nonexponential (see Figure 7), whereas Li et al.[44] found acceptable agreement between the experimental traces and the exponential fitting curves. However, the deviations observed in Figure 7 between simulated time traces and first-order kinetics fall within the experimental error of the analytical method used by Li et al. The first-order rate constants obtained from the exponential fits are listed in Table 1. Whereas the agreement between experimental and simulated rate constants is satisfactory for the smallest bead size, there are significant deviations for the two larger bead sizes. Obviously, the reduction in reaction rate for the largest bead ($d = 320$ μm), as compared to the smaller bead sizes, is too strong to be ascribed solely to the increased bead diameter. Nevertheless, the agreement between simulated and experimental bead-size dependence of the rate constants is reasonable, especially when the variations between the different resins (e.g., in loading with amino groups) and the uncertainties in the input parameters (e.g., the diameters of the *swollen* beads) as well as in the experimental results (e.g., inaccuracies related to start and stop procedures) are taken into account.

The rates of the Knorr attachment reaction observed for PEG-containing resins are much higher than those obtained for the polystyrene resins (Table 1). The results of the simulations are also given in Table 1. These values for k and D_S should not be taken too literally, because other combinations of k and D_S yield very similar first-order rate constants k' for the overall reaction. However, some general trends in the data should be noted. The diffusion coefficient D_S in all of the PEG resins must be larger than that obtained for the polystyrene resin ($D_S = 7 \times 10^{-8}$ cm^2 s^{-1}), because otherwise, the simulated reaction rates are always smaller than the experimental ones, independent of the value inserted for the rate constant, k. Not only D_S but also the second-order rate constant, k, is affected by the resin type, as becomes clear from the simulation of the reaction rate of the Champion resin, which undergoes the fastest Knorr attachment. To reproduce the experimental reaction rate by simulation, the second-order rate constant must exceed $k = 3.5$ M^{-1} s^{-1}, even if $D_S = 3 \times 10^{-6}$ cm^2 s^{-1} is inserted for the diffusion coefficient of the Knorr linker.

6. Modeling of Enzyme-Catalyzed Reactions. Simulations of polymer-supported reactions may also be extended to catalytic reactions, as illustrated by the following example. The kinetics of a typical enzymatic reaction in homogeneous solution are usually described by the Michaelis−Menten (MM) (Scheme 2) reaction, where enzyme R and reactant S form an intermediate Z, which decays either to the reactants S and R or to product P and enzyme R. In matrix-supported reactions in which the enzymes are entrapped in a sol−gel or polymer matrix, both MM[46] and non-MM kinetics[47] have been observed.

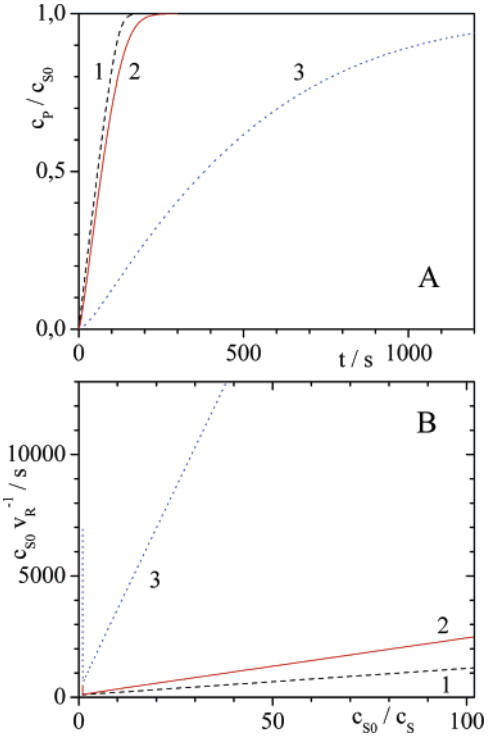

Figure 8. (A) time traces of product formation (expressed in terms of conversion of substrate, c_P/c_{S0}) during the catalytic reaction of Scheme 2. The following parameters were used in the simulation: $k_1 = 10^6$ M^{-1} s^{-1}, $k_{-1} = 10^3$ s^{-1}, $k_2 = 10$ s^{-1}, $c_{S0} = 0.01$ M, $c_{K0} = 10^{-5}$ M, $d = 100$ μm, $X = 0.5$. Curve 1, $D = 10^{-6}$ cm^2 s^{-1}; curve 2, $D = 5 \times 10^{-8}$ cm^2 s^{-1}; curve 3, $D = 10^{-9}$ cm^2 s^{-1}. (B) Lineweaver−Burke plots of the traces shown in part A.

6.1. Effect of *k* and *D* on the Kinetics of Catalytic Reactions. In the polymer-supported model reaction considered here (Scheme 2), the enzyme is assumed to be completely immobilized in the polymer bead, whereas both substrate S and product P are mobile (for the sake of simplicity, the same diffusion coefficient is chosen for S and P). At the beginning of the reaction, no substrate S is present in the resin beads. After the start of the reaction, S diffuses into the resin bead and reacts with the enzyme R, according to eqs I, IV, and V. The product, P, partitions between the bead and the liquid phase. Figure 8 shows the time traces of product formation for two extreme values of the diffusion coefficients, D_S and D_P, but otherwise equal reaction conditions. For the relatively large diffusion coefficient of $D = 10^{-6}$ cm^2 s^{-1}, the kinetics of the polymer-supported reaction are very similar to those of the reaction in homogeneous solution. For example, the reaction rate is of zeroth-order at the beginning of the reaction. The Lineweaver−Burke plot (Figure 8b) of this reaction is linear in good approximation, except for a short induction period at $t < 5$ s. This induction period is needed to establish a more or less homogeneous concentration of S throughout the bead (Figure 9). The maximum reaction rate obtained from the Lineweaver−Burke plot, $v_{R,max}$, is practically the same as in homogeneous solution ($v_{R,max} = 10^{-4}$ M s^{-1}), and the Michaelis−Menten (MM) constant of $K_M = 1.09 \times 10^{-3}$ M exceeds that of the corresponding homogeneous reaction ($K_M = 1.01 \times 10^{-3}$ M) only slightly. For the parameters used in this example, the effect of diffusion on the overall reaction rate is rather modest. Even upon reduction of the diffusion coefficient to

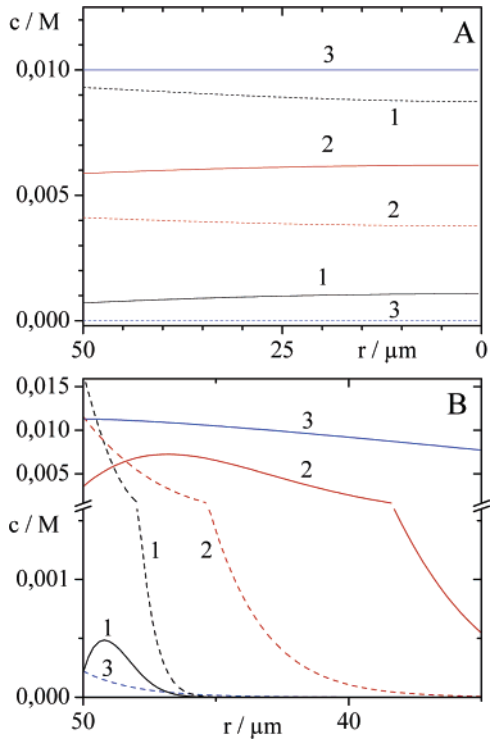

Figure 9. Concentration profiles (concentrations vs distance, r, from the center of the bead) for the catalytic reactions of Figure 8 ($k_1 = 10^6$ M^{-1} s^{-1}, $k_{-1} = 10^3$ s^{-1}, $k_2 = 10$ s^{-1}, $c_{S0} = 0.01$ M, $c_{R0} = 10^{-5}$ M, $d = 100$ μm, $X = 0.5$). Solid lines, c_P; broken lines, c_S. (A) $D = 10^{-6}$ cm^2 s^{-1}; (1) $t = 10$ s, (2) $t = 70$ s, (3) $t = 220$ s. (B) $D = 10^{-9}$ cm^2 s^{-1}; (1) $t = 10$ s, (2) $t = 220$ s, (3) $t = 1720$ s.

$D = 5 \times 10^{-8}$ cm^2 s^{-1}, $v_{R,max}$ remains almost unchanged, and the MM constant is increased to only $K_M = 2.9 \times 10^{-3}$ M.

For very small diffusion coefficients, for example, $D = 10^{-9}$ cm^2 s^{-1}, the overall reaction rate is reduced significantly as compared to the corresponding homogeneous case. Concomitantly, the time traces of product formation do not show zeroth-order rate behavior any more (Figure 8). The Lineweaver−Burke plot (Figure 8b) exhibits a fairly linear relationship for $t > 220$ s, from which $v_{R,max} = 3.5 \times 10^{-5}$ M s^{-1} and $K_M = 0.33$ M is obtained. During the induction period ($t < 220$ s), diffusion is faster than reaction; i.e., the concentration profile of S progresses into the bead. For $t > 220$ s, consumption of S is faster than diffusion; i.e., the concentration of S decreases continuously all over the bead (Figure 9). It is interesting to note that the catalytic centers in the center of the bead, that is, at $r < 40$ μm practically do not participate in the reaction.

6.2. Bead Size Dependence of Catalytic Reactions. To investigate the bead-size dependence of catalytic reactions, two MM-type polymer-supported reactions with different diffusion coefficients but otherwise equal kinetic parameters were simulated. The concentration of S in solution was kept constant during the reaction. The resulting concentration profiles are shown in Figure 10a and b. In the case of rapid diffusion (Figure 10a), almost no bead-size dependence is observed for realistic bead sizes, because the beads are penetrated by the mobile reactant before significant amounts of product have been produced. In the case of slow diffusion (Figure 10b), practically linear concentration gradients of S are formed, which approach a constant value after $t \approx 220$ s. Under these conditions, the reaction rate is determined by the rate of diffusion of S into the beads, which in turn is proportional to the concentration gradient. Accordingly, the time traces of product formation obey zeroth-order kinetics. As the reaction reaches a stationary state after a short induction period, the bead diameter dependence for this reaction is predicted by the Thiele model. Rewriting eq 1 to

$$\mathrm{TM} = \frac{d}{2}\sqrt{\frac{v_R}{D_S c_S^{\,0}}} \tag{6a}$$

and inserting the MM expression

$$v_R = \frac{k_2 k_1 c_R^{\,0}}{k_1 + \dfrac{k_2 + k_{-1}}{c_S^{\,0}}} \tag{6b}$$

for the reaction rate v_R, we obtain

$$\mathrm{TM} = \frac{d}{2}\sqrt{\frac{k_1 k_2 c_R^{\,0}}{D_S c_S^{\,0}\left(k_1 + \dfrac{k_2 + k_{-1}}{c_S^{\,0}}\right)}} \tag{6c}$$

Insertion of the parameters used in Figure 10b yields TM $\approx$ 2 for a bead diameter of $d = 5$ μm.

Inspecting Figure 10d shows that according to the simulations, the reaction rate is proportional to reciprocal bead size for bead diameters $d > 20$ μm, whereas for $d < 5$ μm, the bead size dependence of the reaction rate is negligible. Thus, the simulation results are in nice agreement with the prediction of the Thiele modulus.

6.3. Rates of Catalytic Reactions in Coated Particles. From inspection of Figure 10d, it is obvious that in the case of slow diffusion, only ~10% of the bead volume is reached by the mobile reactant S. Thus, coating of the active resin material onto an inactive core will allow reduction of the amount of applied catalyst appreciably without really affecting the reaction rate. Table 2 summarizes the results of simulations using the same parameters as for the strongly diffusion-controlled reaction of Figure 10b, but restricting the catalytically active region to an active shell coated onto an inactive and impermeable core. As evident from Table 2, reducing the active region of the 100-μm sphere to a shell of 2 μm in thickness saves almost 90% of the catalyst while decreasing the reaction rate by only 10%.

In general, the effect of coating may be assessed by solving eq 6 for the bead radius, $d/2$, which then represents an estimate for the optimum coating thickness.

Effects of Spatial and Temporal Variations of Bead Properties on Overall Reaction Rates. Heterogeneity of the reaction environment and restricted space are features which are inherent to polymer-supported reactions. These features are responsible for many undesired results, which have been described in the literature. Examples are decreasing overall reaction rates during the reaction[23] and broad product distributions in peptide synthesis.

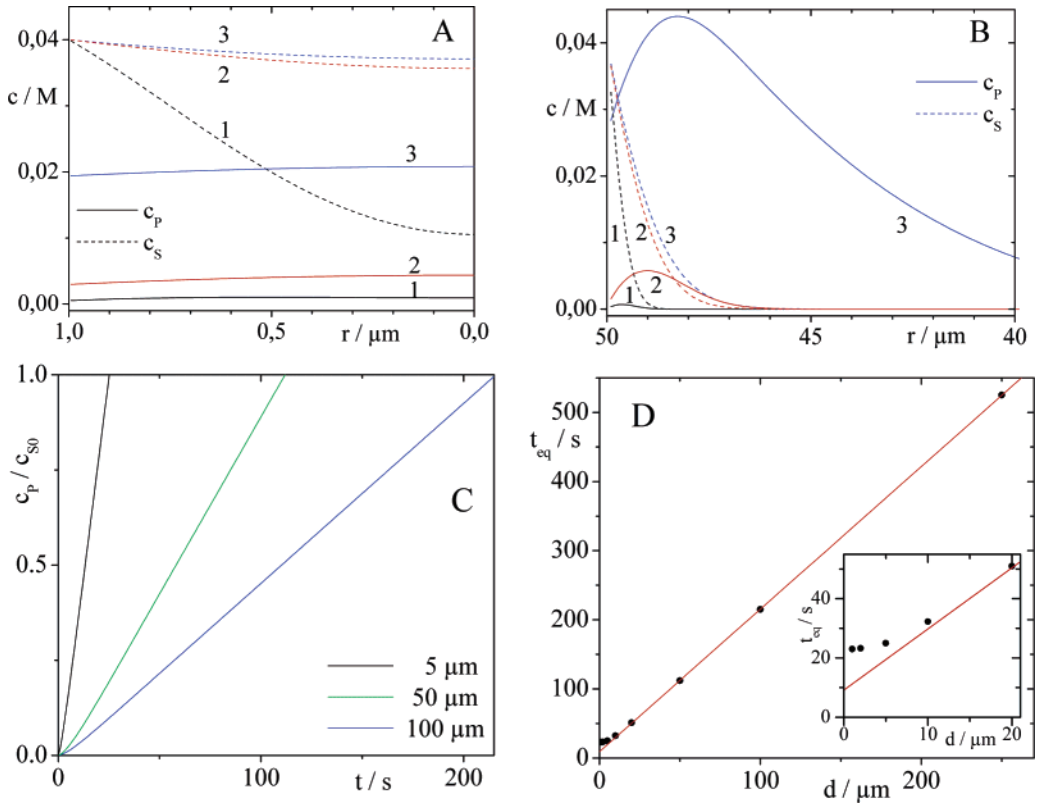

Figure 10. Concentration profiles of substrate (c_S, broken lines) and product (c_P, solid lines) for two catalytic reactions with different diffusion coefficients but otherwise identical parameters ($k_1 = 10^6$ M^{-1} s^{-1}, $k_{-1} = 10^3$ s^{-1}, $k_2 = 10$ s^{-1}, $c_S = c_{S0} = 0.02$ M, $c_{R0} = 10^{-4}$ M, $X = 0.5$) (A) $D = 10^{-6}$ cm^2 s^{-1}; (1) $t = 10$ s, (2) $t = 70$ s, (3) $t = 220$ s. (B) $D = 10^{-9}$ cm^2 s^{-1}; (1) $t = 10$ s, (2) $t = 220$ s, (3) $t = 1720$ s. (C) Time traces of product formation (given as the fraction of reacted substrate, c_P/c_{S0}) for the catalytic reaction of part B. (D) Dependence on bead diameter of reaction times needed for reaching $c_P/c_{S0} = 1$, for the catalytic reaction of part B.

Table 2. Effect of Coating Thickness, d_{coat}, on Reaction Rate[a]

d_{coat}, µm	t_{eq}, s	$n_R/n_{R,max}$[b]
1	421	0.059
2	237	0.115
5	216	0.271
50	216	1

[a] t_{eq} is the reaction times required for production of $c_P = c_S^0$. [b] $n_R/n_{R,max}$ is the fraction of the amount of catalyst required for homogeneous loading of the sphere.

In terms of the model presented above, heterogeneity results in distributions of diffusion coefficients, of second-order rate constants, or both.

1. Distributions of Reaction Rates. Here, we will limit ourselves to the demonstration of the effect of distributions of the second-order rate constant, k, on the overall reaction rate. For this purpose, we define a distribution of immobilized reaction sites (which is the same for all shells, j), by assigning a different value of k to each of these sites. (see eqs VI and VII). For the examples simulated by eqs IX and presented in Figure 11, the distribution of k is assumed to be Gaussian, with a width of $\sigma = 0.625\ k_0$ for all shells $j = 1$ to j_{max} (see the inset in Figure 11A). This is a relatively broad distribution which is more typical of silica based sol−gel materials than of organic resins.[23,37] The most striking result is the incomplete consumption of the polymer-supported reaction centers, R. The chosen width of the distribution renders ~6% of R nonreactive. The time traces deviate clearly from pseudo-first-order kinetics. However, the deviation is hardly measurable for reaction progresses of $c_P/c_{R0} < 0.5$. As to be expected from the preceding discussions, the effect of distribution of rate constants is more pronounced for reactions for which the overall rate is determined by the reaction between S and R. It is less pronounced for reactions for which the rate is controlled by the uptake of S from solution (compare Figure 11a and b).

2. Concentration-Dependent Diffusion Coefficients. There are many reports in the literature about a significant decrease of the overall reaction rate in polymer-supported synthesis when the reactions come close to completion.[23] Recently, it has been shown for reactions in silica-based sol−gel materials, for which diffusion coefficents are $D_S \approx 10^{-10}$−10^{-8} cm^2 s^{-1},[23,37] that the diffusion coefficients decrease significantly as the reaction proceeds.[23] The reason for this decrease is the reduction of free volume in the polymer upon binding of the reactant S to the polymer-supported reactant R. This effect is more pronounced for silica-based materials with their small pore volumes than for organic resins. However, also in the latter, decreasing overall reaction rates are sometimes observed during the reaction, especially in peptide synthesis, during which the growing peptide chains gradually fill up a significant fraction of the initially available free volume.

In swollen polymers, the relation of Mackie and Meares[17,48] is frequently used to describe the dependence of diffusion coefficients on the fraction of free volume; however, for our calculations, we will use eq X to describe the dependence of the diffusion coefficient D_S (j, t) on product concentration

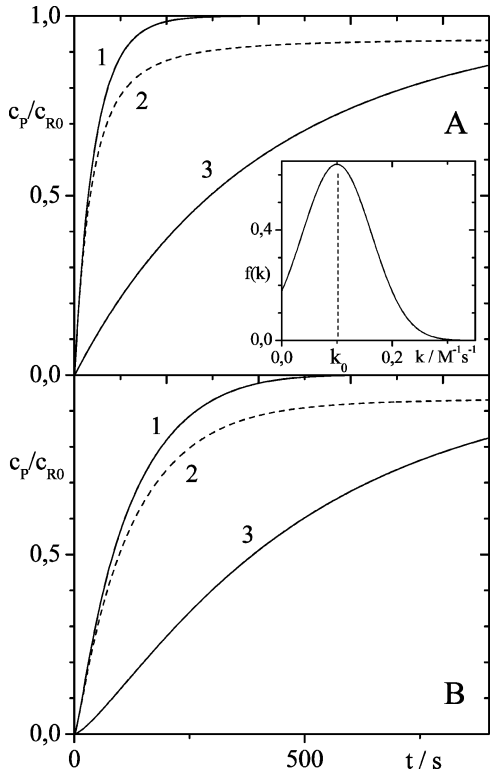

Figure 11. Effect of distribution of second-order rate constants on the overall reaction rate. The time traces of product formation (conversion of polymer-supported reactant, c_P/c_{R0}, vs time) are calculated using the following values for the second-order rate constants: (1) $k = 0.1$ M^{-1} s^{-1}, (2) Gaussian distribution of k as calculated from eq VII using $k_0 = 0.1$ M^{-1} s^{-1} and $\sigma = 0.625k$, (3) $k = 0.01$ M^{-1} s^{-1}. The other parameters are $d = 100$ μm, $X = 0.5$, $c_{R0} = 0.05$ M, $c_{S0} = 0.25$ M, $D_S = 10^{-6}$ cm^2 s^{-1} (A), and $D_S = 10^{-8}$ cm^2 s^{-1} (B). The inset shows the Gaussian distribution, $f(k)$, of the second-order rate constant used in the simulations.

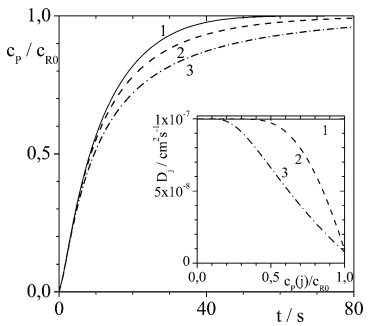

Figure 12. Effect of decrease of diffusion coefficient D_S during reaction progress on the overall reaction rate. The normalized time traces of product formation (conversion of polymer-supported reactant, c_P/c_{R0}, vs time) are calculated for the parameters $k = 1$ M^{-1} s^{-1}, $c_{S0} = 0.25$ M, $c_{R0} = 0.05$ M, $d = 100$ μm, and $X = 0.5$. The concentration dependences of the diffusion coefficients $D_S(j)$ used in the simulations are shown in the inset. The concentration dependences of the diffusion coefficients were calculated using eq VII and the following parameters: (1) $A = 0$; (2) $A = 35$, $B = 3.65$; and (3) $A = 2.5$, $B = 1$ (the numbering in the inset corresponds to the numbering in the main graph).

because it reproduces the data obtained on silica based polymer matrixes[23] better than the Meares equation.

The examples in Figure 12 illustrate the effect of reducing D_S on the progress of the reaction. The concentration dependence of D_S used in these simulations is similar to that observed during the aminomethylation of modified porous silica particles.[23] The reaction rate decreases significantly toward the end of the reaction due to the reduction of the diffusion coefficient to only 10% of its initial value. The effects of rate constant distribution and concentration-dependent diffusion coefficients are hard to distinguish experimentally and often are present simultaneously. They may be distinguished by varying the bead size. The effect of concentration dependence of D_S will become more pronounced with increasing bead size, whereas the effect of the reaction rate distribution remains unaffected. This is illustrated by the results presented in Table 3. Upon increasing the bead diameter from $d = 100$ to 250 μm, the reaction time, t_{90}, for 90% completion increases by a factor of 4.0 for regular beads but only by a factor of 3.5 for resin beads with a Gaussian distribution of second-order rate constants. However, for resin beads with concentration-dependent diffusion coefficients D_S, t_{90} increases by a factor of ~14.

Table 3. Reaction Times (s) for 90% Conversion of R for Regular Beads,[a] Beads with Gaussian Distribution of Second Order Rate Constants,[b] and Beads with Concentration-Dependent Diffusion Constants[c]

t_{90}, s	$d = 100$ μm	$d = 250$ μm
regular bead	27	108
k-site-dependent	45	156
D-concentration-dependent	48	682

[a] $D_S = 10^{-7}$ cm^2 s^{-1}, $k_0 = 1$ M^{-1} s^{-1}, $c_{S0} = 0.25$ M, $c_{R0} = 0.05$ M). [b] $k(u)$ ($\sigma = 0.625k_0$). [c] $D_S(c_P)$ ($A = 2.5$, $B = 1$).

Computational Section

Simple Second-Order Reactions (k and D_S Time- and Space-Independent). The concentration change of S due to diffusion is given by

$$\Delta c_{S,diff}(j,t) = \frac{D_S \Delta t}{V_j \Delta r}[A_j\{c_S(j-1,t) - c_S(j,t)\} - A_{j+1}\{c_S(j,t) - c_S(j+1,t)\}] \quad \text{(Ia)}$$

where Δr is the thickness of the shells, V_j is the volume of shell j, and A_j and A_{j+1} are the outer and inner surface areas of shell j, respectively. The diffusion coefficient D_S is the same for all shells j.

Partitioning of the mobile reactant S between bead resin and solution is considered by introducing the partition coefficient $\alpha_S = c^{eq}_{S,bead}/c^{eq}_{S,sol}$ (where $c^{eq}_{S,bead}$ and $c^{eq}_{S,sol}$ are the equilibrium concentrations of S in bead and solution, respectively) into the difference equations for diffusive concentration changes in solution ($j = 0$) and in the outermost bead shell ($j = 1$).

$$\Delta c_{S,diff}(0,t) = -\frac{D_S \Delta t}{V_0 \Delta r}[A_1\{\alpha_S c_S(0,t) - c_S(1,t)\}] \quad \text{(Ib)}$$

$$\Delta c_{S,diff}(1,t) = \frac{D_S \Delta t}{V_1 \Delta r}[A_1\{\alpha_S c_S(0,t) - c_S(1,t)\} - A_2\{c_S(1,t) - c_S(2,t)\}] \quad \text{(Ic)}$$

The concentration change of S due to chemical reaction is given by eq II.

$$\Delta c_{S,react}(j, t) = -kc_S(j, t)c_R(j, t)\Delta t \quad \text{(II)}$$

The total concentrations of S and R are given by eqs III.

$$c_S(j, t + \Delta t) = c_S(j, t) + \Delta c_{S,diff}(j, t) + \Delta c_{S,react}(j, t) \quad \text{(IIIa)}$$

$$c_R(j, t + \Delta t) = c_R(j, t) + \Delta c_{S,react}(j, t) \quad \text{(IIIb)}$$

Enzymatic Reactions. For the polymer-supported enzymatic reaction given by Scheme 2, the following set of difference equations applies:

The diffusion of the mobile substrate S is described by eqs I. The corresponding expression for the diffusion of the mobile product P is formally obtained by replacing all indexes S in eqs I with P.

The concentration changes due to chemical reaction of S, the immobilized enzyme R, and the product P are given by eqs IV.

$$\Delta c_{S,react}(j, t) = [-k_1 c_S(j, t)c_R(j, t) + k_{-1}c_Z(j, t)]\Delta t \quad \text{(IVa)}$$

$$\Delta c_{R,react}(j, t) = [-k_1 c_S(j, t)c_R(j, t) + (k_{-1} + k_2)c_Z(j, t)]\Delta t \quad \text{(IVb)}$$

$$\Delta c_{P,react}(j, t) = k_2 c_Z(j, t)\Delta t \quad \text{(IVc)}$$

The concentrations of S, R, of the intermediate Z, and of P in shell j at time t are given by eqs V.

$$c_S(j, t + \Delta t) = c_S(j, t) + \Delta c_{S,diff}(j, t) + \Delta c_{S,react}(j, t) \quad \text{(Va)}$$

$$c_P(j, t + \Delta t) = c_P(j,t) + \Delta c_{P,diff}(j, t) + \Delta c_{P,react}(j,t) \quad \text{(Vb)}$$

$$c_Z(j, t + \Delta t) = c_Z(j, t) - \Delta c_{R,react}(j, t) \quad \text{(Vc)}$$

$$c_R(j, t + \Delta t) = c_R(j, t) + \Delta c_{R,react}(j, t) \quad \text{(Vd)}$$

Second-Order Reactions with Space-Dependent Reaction Rate Constants and Concentration-Dependent Diffusion Coefficients. 1. Space-Dependent Reaction Rate Constants. Distributions of reaction rates are considered by defining a Gaussian distribution of polymer-supported reactive sites $R(j, u)$ in shell j,

$$c_R(j, u, 0) = \frac{c_R(j, 0)e^{-(k(u)-k_0)^2/2\sigma^2}}{\sum_u e^{-(k(u)-k_0)^2/2\sigma^2}} \quad \text{(VI)}$$

each site, u, having its own second-order rate constant $k(u)$. The $k(u)$ are obtained as a series of equidistant rate constants $k(u)$ around the central value of k_0.

$$k(u) = k_0[1 - \sigma(u - u_{max}/2)] \quad \text{(VII)}$$

The concentration changes of the reactants are obtained from

$$\Delta c_R(j, u, t) = -k(u)c_S(j, t)c_R(j, u, t)\Delta t \quad \text{(VIIIa)}$$

$$\Delta c_R(j, t) = \Delta c_{S,react}(j, t) = -\Delta c_{P,react}(j, t) = \sum_u \Delta c_R(j, u, t) \quad \text{(VIIIb)}$$

The total concentrations are calculated from

$$c_S(j, t + \Delta t) = c_S(j, t) + \Delta c_{S,diff}(j, t) + \Delta c_{S,react}(j, t) \quad \text{(IXa)}$$

$$c_P(j, t + \Delta t) = c_P(j, t) + \Delta c_{P,diff}(j, t) + \Delta c_{P,react}(j, t) \quad \text{(IXb)}$$

$$c_R(j, u, t + \Delta t) = c_R(j, u, t) + \Delta c_{R,react}(j, u, t) \quad \text{(IXc)}$$

2. Concentration-Dependent Diffusion Coefficients. Due to the concentration dependence of the diffusion coefficient, the effective rate constant of the polymer-supported reaction is rendered time-dependent. Equation X describes the dependence of the diffusion coefficient $D_S(j, t)$ in shell j on the local product concentration $c_P(j)$.

$$D_S(j, t) = D_S(1 - Ae^{-Bc_{R0}/c_P(j,t)}) \quad \text{(X)}$$

c_{R0} is the initial concentration of immobilized reactant R, D_S is the diffusion coefficient for $c_P(j) = 0$, and A and B are two empirical constants.

Conclusions

The presented algorithm allows for the complete modeling of reactions in spherical volumes. On the basis of diffusion coefficient and reaction rate, the reaction progress and the spatial product distribution of a reaction can be predicted. Experimental data on polymer-supported reactions were successfully used to verify the model and allow for the determination of experimentally inaccessible parameters by fitting to the model.

The simulations described above show that two limiting cases exist for reactions in spherical compartments: diffusion and activation control. Activation-controlled reactions show no dependence of the reaction rates on bead size. The concentration dependence of their kinetics is very similar to that in homogeneous solution. The product distribution is homogeneous throughout the beads at all times.

Diffusion-controlled reactions show a strong dependence of the reaction rate, υ_R, on bead diameter, d. For catalytic transformations of mobile substrate at immobilized catalysts, $\upsilon_R \propto d^{-1}$ is found, whereas for the reaction of polymer-supported reactants with mobile reactants, $\upsilon_R \propto d^{-2}$ is valid. In the latter case, sharp reaction fronts are formed during the reaction, which allows radial patterning of the resin beads.

The limit between diffusion and activation control is given by the modulus $kc_Rd^2/500D_S$. If the modulus significantly exceeds unity, the reaction is activation-controlled; otherwise, it is more or less diffusion-controlled.

The rate laws of the two extreme cases can be described by either reaction kinetics in homogeneous solutions or by the kinetics of diffusion into spheres. The algorithm described above allows quantitative modeling also of intermediate cases under practically any boundary conditions, providing the spatial product distributions at arbitrary times.

The algorithm requires as input parameters the diffusion coefficient, D_S; the rate constant, k, within the resin bead; the bead diameter, d; the volume fraction occupied by the spheres, X; the concentrations of the species involved in the reaction; and the partition coefficient, α_S; of the mobile reactant between resin and solution. If all of these parameters

have been determined (e.g., by spectroscopic methods[37,49−53]), the algorithm should be able to reproduce experimental reaction kinetics quantitatively. However, D_S, k, and α_S are often difficult to determine. If at least one of these three parameters can be obtained by an independent method (most probably D_S[32] and α_S[4]), the others may be calculated or at least estimated with the help of the model algorithm. Thus, the algorithm, in addition to its practical value in the planning of syntheses, may also help to get a deeper insight into the physical chemistry of resin-supported reactions.

Acknowledgment. The authors gratefully acknowledge support from the DFG graduate college "Chemistry in Interphases". Lars Poulsen is acknowledged for helpful discussions. The software described and applied in this article are offered as Excel or Matlab files and will be sent to interested readers free of charge.

References and Notes

(1) Walsh, D.; Wu, D.; Chang, Y.-T. *Curr. Opin. Chem. Biol.* **2003**, *7*, 353−361.
(2) Hudson, D. J. *J. Comb. Chem.* **1999**, *1*, 333−360, 402−457.
(3) Sherrington, D. C. *Chem. Commun.* **1998**, 2275−2286.
(4) Yan, B.; Fell, J. B.; Kumaravel, G. *J. Org. Chem.* **1996**, *61*, 7467−7472.
(5) Rademann, J.; Barth, M.; Brock, R.; Egelhaaf, H.-J.; Jung, G. *Chem.—Eur. J.* **2001**, *7*, 3884−3889.
(6) Kress, J.; Zanaletti, R.; Rose, A.; Frey, J. G.; Brocklesby, W. S.; Ladlow, M.; Bradley, M. *J. Comb. Chem.* **2003**, *5*, 28−32.
(7) Li, W.; Yan, B. *J. Org. Chem.* **1998**, *63*, 4092−4097.
(8) Vaino, A. R.; Janda, K. D. *J. Comb. Chem.* **2000**, *2*, 579−596.
(9) Li, W.; Czarnik, A. W.; Lillig, J.; Xiao, X.-Y. *J. Comb. Chem.* **2000**, *2*, 224−227.
(10) Kueppers, M.; Heine, C.; Han, S.; Stapf, S.; Bluemich, B. *Appl. Magn. Reson.* **2002**, *22*, 235−246.
(11) Gotfredsen, C. H.; Grøtli, M.; Willert, M.; Meldal, M.; Duus, J. Ø. *J. Chem. Soc., Perkin Trans. 1* **2000**, 1167−1171.
(12) Thiele, E. W. *Ind. Eng. Chem.* **1939**, *31*, 916−920.
(13) Helfferich, F. *J. Am. Chem. Soc.* **1954**, *76*, 5567−5568.
(14) Smith, N. L.; Amundson, N. R. *Ind. Eng. Chem.* **1951**, *43*, 2156−2167.
(15) Roucis, J. B.; Ekerdt, J. G. *J. Catal.* **1984**, *86*, 32−47.
(16) Tan, H. K. S. *Chem. Eng. Sci.* **1989**, *44*, 2760−2762.
(17) Biffis, A.; Corain, B.; Cvengrošová, Z.; Hronec, M.; Jeřábek, K.; Králik, M. *Appl. Catal., A* **1996**, *142*, 327−346.
(18) Bacha, S.; Montagne, M.; Bergel, A. *AlChE J.* **1996**, *42*, 2967−2976.
(19) Cioci, F.; Lavecchia, R. In *Handbook of Nonmedical Applications of Liposomes*; Lasic, D. D., Barenholz, Y., Eds.; CRC: Boca Raton, 1996; Vol. 3, pp 287−316.
(20) Králik, M.; Fišera, R.; Zecca, M.; d'Archivio, A. A.; Galantini, L.; Jeřábek, K. *Collect. Czech. Chem. Commun.* **1998**, *63*, 1074−1088.
(21) Jauregui-Haza, U. J.; Pardillo-Fontdevila, E.; Kalck, P.; Wilhelm, A. M.; Delmas, H. *Catal. Today* **2003**, *79*−*80*, 409−417.
(22) Maiwald, M.; Fischer, H. H.; Kim, Y.-K.; Albert, K.; Hasse, H. *J. Magn. Reson.* **2004**, *166*, 135−146.
(23) Walcarius, A.; Etienne, M.; Bessière, J. *Chem. Mater.* **2002**, *14*, 2757−2766.
(24) Riley, M. R.; Muzzio, F. J.; Reyes, S. C. *Comput. Chem. Eng.* **1998**, *22*, 525−534.
(25) Trotta, A.; Del Giudice, S. *Compu. Chem. Eng.* **1985**, *9*, 167−173.
(26) Wadiak, D. T.; Hight, T. K. *J. Spacecr. Rockets* **2003**, *40*, 584−590.
(27) Kress, J.; Rose, A.; Frey, J. G.; Brocklesby, W. S.; Ladlow, M.; Mellor, G. W.; Bradley, M. *Chem.—Eur. J.* **2001**, *7*, 3880−3884.
(28) Doraiswamy, L. K.; Sharma, M. M. *Heterogeneous Reaction, Analysis, Examples, and Reactor Design*; Wiley-Interscience: New York, 1984, Vol 2.
(29) Rapp, W. E. Ph.D. Thesis, University of Tübingen, Germany, 1985.
(30) Wagner, M. L.; Scheraga, H. A. *J. Phys. Chem.* **1956**, *60*, 1067−1076.
(31) Terazima, M.; Okamoto, K.; Hirota, N. *J. Phys. Chem.* **1993**, *97*, 5188−5192.
(32) Masaro, L.; Zhu, X. X. *Prog. Polym. Sci.* **1999**, *24*, 731−775.
(33) Yamane, Y.; Matsui, M.; Kimura, H.; Kuroki, S.; Ando, I. *J. Appl. Polym. Sci.* **2003**, *89*, 413−421.
(34) Kapur, V.; Charkoudian, J.; Anderson, J. L. *J. Membr. Sci.* **1997**, *131*, 143−153.
(35) Rigler, R.; Mets, U.; Widengren, J.; Kask, P. *Eur. Biophys. J.* **1993**, *22*, 169−175
(36) Groth, T.; Grøtli, M.; Meldal, M. *J. Comb. Chem.* **2001**, *3*, 461−468.
(37) McCain, K. S.; Hanley, D. C.; Harris, J. M. *Anal. Chem.* **2003**, *75*, 4351−4359.
(38) Holder, E.; Oelkrug, D.; Egelhaaf, H.-J.; Mayer, H.; Lindner, E. *J. Fluoresc.* **2002**, *12*, 383−395.
(39) Farrer, R. A.; Copeland, G. T.; Previte, M. J. R.; Okamoto, M. M.; Miller, S. J.; Fourkas, J. T. *J. Am. Chem. Soc.* **2002**, *124*, 1994−2003.
(40) Yadav, G. D.; Haldavanekar, B. V. *React. Funct. Polym.* **1997**, *32*, 187−194.
(41) Belyaev, S. V.; Vainshtein, E. F.; Klyuev, M. V. *Kinet. Catal.* **1992**, *43*, 245−248.
(42) Tomoi, M.; Ford, W. T. *J. Am. Chem. Soc.* **1981**, *103*, 3821−3828.
(43) Balakrishnan, T.; Ford, W. T. *J. Org. Chem.* **1983**, *48*, 1029−1035.
(44) Crank, J. *The Mathematics of Diffusion*, 2nd ed.; Clarendon Press: Oxford, 1975.
(45) Li, W.; Xiao, X.; Czarnik, A. W. *J. Comb. Chem.* **1999**, *1*, 127−129.
(46) Shabat, D.; Grynszpan, F.; Saphier, S.; Turniansky, A.; Avnir, D.; Keinan, E. *Chem. Mater.* **1997**, *9*, 2258−2260.
(47) Braun, S.; Rappoport, S.; Zusman, R.; Avnir, D.; Ottolenghi, M. *Mater. Lett.* **1990**, *10*, 1−5.
(48) Mackie, J. S.; Meares, P. *Proc. R. Soc. London, A* **1955**, *232*, 498−509.
(49) Lehr, B.; Egelhaaf, H.-J.; Fritz, H.; Rapp, W.; Bayer, E.; Oelkrug, D. *Macromolecules* **1996**, *29*, 7931−7936.
(50) Lehr, B.; Egelhaaf, H.-J.; Rapp, W.; Bayer, E.; Oelkrug, D. *J. Fluoresc.* **1998**, *8*, 171−177.
(51) Egelhaaf, H.-J.; Oelkrug, D.; Herman, P.; Holder, E.; Mayer, H. A.; Lindner, E. *J. Mater. Chem.* **2001**, *11*, 2445−2552.
(52) Mahurin, S. M.; Dai, S.; Barnes, M. D. *J. Phys. Chem. B* **2003**, *107*, 13336−13340.
(53) Ulijn, R. V.; Brazendale, I.; Margetts, G.; Flitsch, S. L.; McConnell, G.; Girkin, J.; Halling, P. J. *J. Comb. Chem.* **2003**, *5*, 215−217.

CC050015Z